2 Raman Instrumentation

Sanford A. Asher and Richard Bormett

Abstract. The last decade has seen major advances in the applications of Raman spectroscopy to materials science. We review here the dramatic improvements in Raman instrumentation that have enabled these incisive studies. This chapter separately discusses advances in lasers, spectrometers, optics and detectors and illustrates some of these advances in a few examples of new applications and instrumentation used in materials science research.

The rapidly increasing use of Raman spectroscopy as a routine method of materials characterization is a direct result of the recent dramatic advances in lasers, detectors and spectroscopic instrumentation [1–3]. Raman instrument companies have rapidly commercialized many of these advances. Some of these advances have made it possible to commercialize new relatively inexpensive instruments (< \$100 K including the laser). This has significantly increased the number of Raman instruments worldwide [4]. The new generation of low cost, high performance Raman instrumentation now makes Raman spectral measurements easy, even for nonexperts. Industrial Raman instruments are now available for real time chemical process monitoring, manufacturing quality control and routine analytical investigations. Many of these industrially rugged instruments utilize fiber optic probes that dramatically simplify measurements making them routine and easy for nonexperts [5].

The Raman instrument advances have also affected the research grade Raman instruments. Research grade instruments are available with extended wavelength coverage from the UV into the near IR spectral regions. A common feature of most of these new research-grade Raman instruments is the incorporation of a microscope. These new Raman microscopes permit spectral imaging of samples with spatial resolutions< 1 mm. The high spatial resolution allows rapid chemical speciation of spatially inhomogeneous samples.

Most Raman instrumentation is fabricated by selecting the appropriate lasers, optics, spectrometers, and detectors necessary to optimize the Raman spectrometer for the required Raman spectral measurements. Thus, it is natural to organize this chapter into separate sections that separately discuss these individual components. The last section will give a few examples of use of new Raman instrumentation in materials science.

2.1.3 Nonlinear Raman Measurements

Raman scattering is a two-photon process [15]. In the case of spontaneous Raman scattering the two photons include the laser excitation photon and a photon from the vacuum field [15]. In most cases CW laser excitation produces only a small number of Raman photons, and this number is negligible compared to the vacuum field photon density. Thus, the Raman intensity is observed to increase linearly with the incident excitation beam intensity. However, if the photon density at the Raman shifted wavelength approaches or exceeds the vacuum field photon density, stimulated Raman scattering will occur. This process shows a higher intensity dependence on the incident beam intensity. This is a rich area of research with numerous important applications in its future. Stimulated Raman scattering as well as the numerous other nonlinear Raman scattering processes will not be discussed here, except to note that high peak-power laser sources are required. These methodologies generally utilize ns to ps pulsed lasers, which give high peak powers at modest pulse energies.

2.2 Choice of Raman Excitation Wavelength

As a high intensity single frequency light source, the laser is an ideal Raman excitation source. The laser excitation frequency is the major determinant of the information content of a Raman spectral measurement. The laser frequency determines the spectral range of the measurement; the operating mode (pulsed or continuous) determines the excitation photon flux, as well as its temporal characteristics. Essentially all Raman measurements are photon limited. Thus, it would appear to be desirable to utilize as bright an excitation source as possible. However, in reality the incident laser power must be constrained such that the focused energy density is below the level that causes sample photochemical or thermal degradation and below the powers that cause nonlinear optical phenomena [16,17]. This represents a major limitation for the use low duty cycle pulsed laser sources. Although they may have an average power identical to that of a CW laser, their much higher peak powers can result in significant nonlinear optical phenomena as well as increased photochemical and photothermal sample damage.

Although the first laser Raman measurements were obtained by using a pulsed Ruby laser in the near IR at 694 nm [6], pulsed laser sources generally have significant pulse-to-pulse energy fluctuations. For scanning Raman instruments this results in low spectral S/N ratios, which are dominated by the standard deviation in the pulse energies.

2.2.1 CW Lasers

The red 632.8 nm CW He–Ne laser was the first laser to be incorporated in commercial Raman instruments [6]. This laser was quickly replaced by the higher power CW Ar^+ and Kr^{++} lasers that have numerous excitation lines in the 350–700 nm region. These CW Ar^+ and Kr^{++} lasers are available with very high powers in many spectral lines (1–5 W) in the visible spectral region. In addition, these lasers can be used to pump jet stream dye lasers to obtain relatively high power excitation continuously tunable throughout the visible spectral region. These dye lasers were mainly utilized for resonance Raman measurements that required excitation wavelength tunability.

More recently near-IR diode lasers [18] around 780 nm as well as diode pumped YAG lasers have become popular because of their low cost, small size, low power consumption and reliability. As discussed below these lasers are being used as the excitation sources for a new generation of inexpensive, small Raman spectrometers that are now being commercialized.

These CW laser sources are ideal for nonabsorbing samples because the laser beam can be focused to a small beam waist in the sample. The small beam waist is ideal for efficient light collection and efficient coupling of the Raman scattered light into the spectrometer. It is possible to use very high irradiances with CW lasers to obtain very high spectral S/N ratios. The maximum irradiance possible is limited by the sample damage threshold and the threshold for the onset of nonlinear optical phenomena. For example, 1 W of CW excitation focused onto a 10 μm^2 area results in a fluence of 10 MW/cm^2 which can be sufficient to induce nonlinear optical processes, such as two-photon absorption followed by heating and sample degradation. Thus, a practical limit exists for the fluence of a CW laser that can be practically used for Raman spectral measurements for "nonabsorbing" samples. For absorbing samples, laser heating causes degradation at much lower incident intensities.

2.2.2 Pulsed Lasers

The increased peak powers of pulsed lasers results in the occurrence of nonlinear optical processes at much smaller average incident laser powers than for CW lasers [16,17]. Thus, pulsed laser sources are generally avoided whenever a CW laser source is available for nonresonance, spontaneous Raman scattering experiments [19].

Until very recently pulsed laser sources were the only means of extending Raman excitation into the UV [19,20]. Nonlinear optical processes such as frequency doubling and mixing in nonlinear crystals such as β-barium borate and KDP generated UV light from dye lasers pumped by Q switched YAG lasers and excimer lasers. For example, the YAG fundamental at 1.06 μm can be frequency doubled to 532 nm or tripled to 355 nm to pump a dye laser. This dye laser can be frequency doubled and mixed with the 1.06 μm YAG fundamental to generate tunable UV excitation from 196 nm to the near IR. Alternatively a XeCl excimer laser [19] at 308 nm can be used to pump a dye laser. The dye laser light can be similarly frequency doubled to provide UV

excitation from 196–350 nm. Using this approach, it is possible to generate light of any wavelength in this UV spectral region.

An alternative approach to obtain UV excitation uses stimulated Raman scattering to shift the laser wavelength [21]. Most often the Raman shifting material used is H_2 gas which shows a $\sim 4200\,cm^{-1}$ Raman transition. It is easy to achieve numerous excitation wavelengths by utilizing a number of anti-Stokes Raman shifts in H_2. For example, 204 nm excitation can be easily obtained from 5 H_2 anti-Stokes Raman shifts of the tripled YAG at 355 nm [21,22]. Numerous additional Raman shifted lines in the UV can also be obtained from the quadrupled YAG line at 266 nm.

A much more convenient CW UV source is obtained by frequency doubling Ar^+ and Kr^{++} lasers. For example, > 200 mW of 244 and 257 nm light can be obtained from intracavity doubled Ar^+ lasers [23], while $\sim$ 30 mW can be obtained at 229 nm, with additional lines occurring between 229 and 257 nm. The intracavity frequency doubled Kr^{++} laser [24] produces a few mW of 206 nm light, which is adequate for most UV Raman measurements. A new hollow cathode UV laser is now emerging [13] that utilizes as the gain medium excited states of metal ions sputtered into the gas phase. These lasers are small, energy efficient and inexpensive. Prototypes of these hollow cathode lasers using Cu and Ag have demonstrated laser excitation at 248 and 224 nm. These lasers operate quasi-CW at $\sim$ 10 kHz repetition rates with average powers of $\sim$ 1 mW, which is adequate for UV-Raman measurements.

2.3 Optical Methods for Rayleigh Rejection

The purpose of the Raman spectrometer is to reject the intense Rayleigh scattered light and to disperse the Raman scattered light into its component frequencies for detection. The relative intensity ratio of Rayleigh to the Raman scattered light is often > 10^9 [6]. With such a large disparity between the Raman and Rayleigh intensities, the Rayleigh light must be greatly attenuated before the spectrograph section of the Raman spectrometer. If the Rayleigh light is allowed to enter the spectrograph unattenuated, it will generate sufficient stray light to obscure all or part of the much weaker Raman spectrum. Preventing intense Rayleigh scattered light levels from entering the spectrograph stage of the Raman spectrometer is the most challenging task for the Raman spectrometer.

A modern Raman spectrometer can utilize a number of different technologies to attenuate the relatively intense Rayleigh scattered light such as holographic notch filters [25], crystalline colloidal array Bragg diffraction filters [26], dielectric filters and multi-stage spectrometers [27]. Instruments that measure Raman bands lying close (< $150\,cm^{-1}$) to the Rayleigh line, utilize more costly, complex and inefficient Rayleigh rejection devices.

A band pass or band reject filter serves as the simplest Rayleigh rejection device. Holographic notch filters are available for the visible and near IR spectral regions; these filters typically permit Raman spectral measurements of frequency shifts greater than $\sim 100\,cm^{-1}$. Low cost dielectric [28] filters suitable for Rayleigh rejection are available from the UV $\sim$ 230 nm [29] through the near IR spectral regions. The hard oxide dielectric filters are suitable for UV Raman spectral measurements within $400\,cm^{-1}$ of the Rayleigh line. However, multistage Raman spectrometers are typically required to routinely measure Raman shifts within $50\,cm^{-1}$ of the Rayleigh line in the visible, and within $200\,cm^{-1}$ with UV excitation.

2.3.1 Holographic Notch Filter

The holographic notch filter [25] selectively rejects (through Bragg diffraction) a narrow band of light, while passing light outside of the band rejection region. The notch filter is constructed in a photosensitive medium, dichromated gelatin, by exposing it to interfering laser beams, which creates a periodic modulation in the refractive index. This periodicity produces a strong 3D Bragg reflection that can efficiently (> 99.9%) diffract away the Rayleigh line, while transmitting adjacent wavelengths with > 90% efficiency. These holographic notch filters are manufactured to have the center (or near center) diffraction wavelength at the Raman excitation frequency. The sharp transition from high diffraction efficiency to high transmission makes the holographic notch filters a nearly ideal Rayleigh rejection filter for Raman measurements close to the Rayleigh line ($100\,cm^{-1}$). Unfortunately holographic notch filters are not yet available for excitation wavelengths shorter than 350 nm. Since each holographic notch filter efficiently operates over only a small wavelength range ($\sim$ 40 nm) numerous filters would be required for Raman measurements throughout the visible and near IR spectral region. However, holographic notch filters are ideal for Raman instruments that operate with only a few laser frequencies.

2.3.2 Dielectric Edge Filters

Raman edge filters [28,29] (typically a dielectric stack or rugate) are a low cost alternative to holographic notch filters for excitation wavelengths from the NIR to the UV. The rugate filter [30] is the dielectric equivalent of the holographic notch filters; the diffracting element is a stack of dielectric coatings with spacings and refractive index modulations sufficient to diffract the desired wavelength. Unfortunately, the current Raman edge filter performance (blocking bandwidth and edge steepness) is still inferior to that of holographic notch filters. The increased blocking bandwidth of the dielectric filters typically obscures Raman bands closer than $\sim 200\,cm^{-1}$ to the Rayleigh line in the visible/near-IR and $\sim 400\,cm^{-1}$ in the UV. In addition, to the increased rejection bandwidth, dielectric filters typically show a $100–200\,cm^{-1}$ periodic ripple in transmittance. The transmittance variation typically requires the use of an instrument intensity correction function for the Raman

spectral measurement. However, the rugate filter technology is still emerging, and it is likely that the rugate filter performance will dramatically improve in the near future.

2.3.3 Pre-monochromator Rayleigh Rejection

Single or double pre-monochromators are the method of last resort for Rayleigh light rejection [27]. These pre-monochromators utilize multiple dispersive elements (gratings) and spatial filters (slits) to reduce the amount of Rayleigh light that reaches successive spectrometer stages. The stray light from the relatively intense Rayleigh scattering is attenuated by 10^3 to 10^5 per monochromator stage. For example if a single stage of a monochromator reduces the stray light by 10^4 then a double monochromator will have a stray light background decrease of 10^8, and a triple monochromator will have a stray light background decrease of 10^{12}. Only double and triple monochromators permit Raman measurements below $50\,\mathrm{cm}^{-1}$.

Unfortunately, the high Rayleigh rejection efficiency of the pre-monochromator stages is accompanied by a loss in light throughput. A triple monochromator will typically have an optical throughput of 3–10% compared to 30–50% for a single monochromator. These inefficient multistage Raman spectrometers survive because they can be used over a broad range of wavelengths and because they can uniquely measure bands close to the laser line.

2.4 Raman Spectrometers

The availability of holographic notch filters and dielectric filters for Rayleigh rejection has allowed the development of simple dispersive and non-dispersive multichannel Raman spectrometers that utilize CCD detectors. The non-dispersive Raman spectrometers separate the Raman scattered light into its component frequencies through electronically or mechanically tunable band-pass filters [31]. Alternatively, an interferometer can be used to construct a Fourier transform Raman spectrometer [9]. This FT-Raman instrument utilizes the same interferometer technology as FT-IR spectrometers. However, for the typical near IR Raman excitation ($\lambda > 900\,\mathrm{nm}$) they utilize a high purity Ge or a GaAs detector. The most common and still most versatile Raman spectrometers still utilize holographic dispersive gratings and CCD multichannel detectors. These spectrometers are useful from the UV to the near IR spectral region.

2.4.1 Dispersive Raman Spectrometers

Dispersive Raman instruments are typically characterized by their optical design. Their figures of merit are given by their light collecting power ($f/\#$),

their dispersion and their optical focal lengths [3]. Dispersive spectrometers may, for example, utilize on axis transmission optics or off axis reflecting optics [2,3]. The focal length of the spectrometer and the ruled line density of the grating determine the ultimate resolution of a dispersive instrument. The most useful spectrometer designs permit easy grating changes with easy wavelength calibration and rescaling of the Raman frequency scale when changing resolution and excitation wavelengths.

Dispersive spectrometers that scan the grating angle to pass different wavelength regions across a slit use a single channel detector, such as a photomultiplier. High precision and high accuracy cosecant scanning drives are required if the spectrometer is to scan linearly in cm^{-1}. Simpler grating drives can be suitable for spectrometers that utilize multichannel detectors if the spectrometer is calibrated at each grating setting; the entire Raman spectrum is acquired without moving the grating. However, high precision grating motion is still required if the spectrometer must be repeatedly reset to a precise orientation in order to repeatedly set a particular wavelength onto a particular pixel of the multichannel detector.

Practical optical considerations typically result in spectrometers with focal lengths between 0.25 m and 1.5 m and grating groove densities between 600 g/mm and 3600 g/mm. The dispersion of the Raman spectrometer is increased by either increasing the spectrometer focal length or increasing the number of lines per millimeter of the grating. Spectrometer resolution is generally increased by increasing the grating groove density rather than increasing the focal length.

Multichannel Raman spectrometers typically sacrifice high resolution for a large spectral window. Table 2.1 shows the typical best resolution of a commercially available 0.25 m focal length multichannel Raman spectrometer for typical laser and grating combinations with a 578 channel detector (resolution is typically limited to 2.5 pixels). Multichannel spectrometers are also available that simultaneously utilize two gratings and a large multichannel detector (1024 elements) to acquire the entire Raman spectrum ($100–3500\,\mathrm{cm}^{-1}$) in a single scan. However, the loss of effective instrument throughput and/or loss of resolution in these instruments may not be acceptable for some applications.

Table 2.1. Typical instrument resolutions (in cm^{-1}) utilizing various grating and laser combinations with a 250 mm focal length spectrometer

Grating (g/mm)			
Wavelength (nm)	2400	1800	1200
780	NA	0.6	1.6
633	0.52	1.5	2.9
514	1.6	2.8	4.9
457	2.4	3.8	6.5

Optimal dispersive Raman instrument performance requires that the spectrometer and Raman collection optics meet three conditions: (1) The spectrometer operate at a slit setting that matches the detector channel size to the spectrometer resolution. (2) The Raman light collection optics magnify the laser spot size at the sample to the entrance slit size (avoid overfilling the slit). (3) The Raman light collection optics match the spectrometer f-number (avoid overfilling the spectrometer optics). The spectrometer optical efficiency and resolution can also be degraded by optical imperfections such as chromatic aberration, astigmatism, and coma. While transmission optics typically minimize astigmatism and coma, chromatic aberration can become a serious problem in the red and blue. Likewise reflective optics avoid chromatic aberrations, but can introduce astigmatism and often coma.

2.4.2 FT-Raman Spectrometers

As the Raman excitation wavelength increases beyond $\sim 850\,\text{nm}$, CCD detectors and detectors, which utilize photocathodes (such as photomultipliers, and intensified CCD and Reticons) become inefficient. Unfortunately, the only useful near IR detectors have high background noise levels [32]. Thus, it is necessary to utilize multiplex techniques to obtain acceptable spectral signal-to-noise ratios. FT-Raman spectrometers are ideally suited for use with diode pumped Nd:YAG lasers operating at 1064 nm. While FT Raman spectrometers would show no increase in S/N for shot noise limited detectors, significant S/N increases occur with the noisy detectors used with near IR Raman excitation. The use of near IR excitation often has the crucial advantage of reducing fluorescence interference. In addition, FT Raman spectrometers have both high spectral resolution and high frequency precision. However, near IR Raman measurements are disadvantaged by the smaller Raman scattering cross sections in the near IR and the poorer performance of the near IR detectors. Table 2.2 compares the main advantages and disadvantages of near IR FT-Raman measurements versus typical visible Raman measurements using dispersive Raman instruments.

2.4.3 Detectors

Until recently photomultipliers were the standard detectors used for Raman spectral measurements. The entire UV, visible to near IR spectral region ($< 900\,\text{nm}$) is well covered with an AlGaAs photocathode which has quantum yields $> 10\%$ over this entire spectral range [32]. When cooled to $-40\,^{\circ}\text{C}$ and used with photon counting detection, these detectors (such as the RCA 1420A-02 PMT) are almost ideal detectors with only a few counts per second of background and a linear dynamic range of $> 10^6$. In fact, PMT detectors are still used for high resolution Raman measurements because they can be masked by a final slit which can be as narrow as a few μm (in contrast to the $\sim 25\,\mu\text{m}$ limits associated with the pixels of CCD and Reticon detectors).

Table 2.2. Relative performance characteristics of dispersive and FT-Raman instruments

Feature	Dispersive Raman	FT-Raman
Available wavelengths	$< 200\,\text{nm}$ to 850 nm	1064 nm (99% systems)
Detector	CCD, shot noise limited	Ge or InGaAs, detector noise limited
Best spectral resolution	typically $1-4\,\text{cm}^{-1}$	$\sim 0.5\,\text{cm}^{-1}$
Fluorescence suppression	moderate at 785 nm, poor at 514 nm, good at 244 nm	Excellent
Operation at elevated temperatures	excellent, $> 1000\,^{\circ}\text{C}$	poor, $< 250\,^{\circ}\text{C}$
Relative υ^4 advantage (from 1064)	@ 785 nm: 3.38 @ 514 nm: 18.3 @ 244 nm: 362	1

Multichannel detectors [1,3] are far superior for lower resolution studies ($> 1\,\text{cm}^{-1}$) because their multiplex advantage increases the spectral signal-to-noise ratios by the square root of the number of resolution elements over a shot-noise limited detector such as a photomultiplier. The selection of a specific CCD camera for Raman spectroscopy requires careful consideration. The wide selection of chip types, pixel sizes and operating temperatures must be considered for background dark count rate, quantum efficiency and read out noise. The scientific CCD detector with a quantum efficiency approaching 70% and very low dark current in the visible is almost ideal for most NIR and visible wavelength Raman studies. With UV Raman the detector quantum efficiency must be enhanced either by depositing UV fluorophores on the CCD surface, or by utilizing a backthinned CCD. However at the lowest light levels, where detector read noise or detector background dominates the S/N ratio, image intensifiers significantly improve the detectivities of CCD arrays.

With UV excitation the advantages of utilizing an intensified CCD typically far outweigh the disadvantages of a decreased detector dynamic range and the increased statistical variance associated with the distribution of gain in the intensifier. Most UV Raman spectral measurements involve a low photon flux. Intensified CCDs are especially helpful to align and set up a Raman measurement; the alignment is guided by observing the real time Raman spectrum. We have found that an intensified CCD array gives significantly higher spectral signal-to-noise values in the UV compared to any unintensified CCD detector.

2.4.4 Imaging Raman Spectrometers

Raman spectroscopy with a microscope is rapidly becoming the method of first choice for Raman analysis. The use of a microscope operating in a 180°

backscattering geometry eliminates the need to continually adjust the laser onto the sample and to focus the scattered light onto the spectrometer. Raman microspectrophotometers utilize research grade microscopes to focus the excitation onto the sample and to collect and transfer the Raman scattered light into the Raman spectrometer. High numerical aperture microscope objectives greatly enhance the spatial resolution and the optical collection power of the Raman instrument. Once aligned, the user is only required to place a sample under the microscope and adjust it for best optical focus. These Raman microscopes are easy to use and are capable of analyzing small areas ($\sim 1\,\mu m^2$) in order to determine the spatial distributions of chemical species.

Traditional Raman images are obtained by translating the sample across the microscopic objective focus with a motorized stage (Raman image mapping) and constructing images from data extracted from each spectrum. However new generations of Raman microscopes are emerging that utilize novel tunable filters to obtain Raman spectral images by illuminating a large field of view, typically 20–200 µm, and analyzing it for one or more specific Raman wavelengths (global Raman imaging) [31].

Commercial global Raman imaging spectrographs are available that use dielectric filters, acousto-optic tunable filters (AOTF) or liquid crystal tunable filters (LCTF). The electronic wavelength tuning ability and high image quality and high spectral resolution ($7–9\,cm^{-1}$) of LCTF devices make them the preferred global imaging dispersing elements, in spite of their lower optical efficiencies (< 20%). Although, dielectric filters have a large throughput (60%) they have a lower resolution ($\sim 15\,cm^{-1}$). Raman imaging spectrometers equipped with liquid crystal tunable filters have been demonstrated to give 250 nm spatial resolution and $7\,cm^{-1}$ spectral resolution.

Still higher spatial resolution (~ 100 nm) is available with the use of a Raman scanning near field optical microscope (RSNOM) [33]. The RSNOM uses a special fiber optic tapered to an aperture less than the optical wavelength to couple the laser light to the sample. The spatial resolution is limited by the size of the aperture, the proximity of the tip to the sample and the excitation wavelength. Coupling the Raman excitation light out of the SNOM tip remains a very inefficient process, and extremely long integration times are required to obtain moderate S/N from very strong Raman scatterers. The best results have been obtained where the RSNOM excitation wavelength is in resonance with an absorption band of the sample producing a resonance Raman spectrum [33].

2.5 Examples of New Raman Instruments for Materials Characterization

In our laboratory we are using UV Raman spectroscopy to investigate the growth and structure of CVD grown diamond [34–36]. One objective is to obtain additional insight into the diamond growth mechanism, in order to optimize the process to increase the rate of diamond growth and to improve CVD diamond quality. With this in mind we built two instruments to examine CVD diamond films. For *ex situ* CVD diamond film studies we built a UV Raman microscope [37] in order to spatially examine the diamond bands to monitor stress, diamond crystal size, and to examine the structure and location of non-diamond impurities within the CVD diamond films. In addition, we built a separate UV Raman instrument to examine *in situ* growing diamond films within a CVD plasma reactor [38].

2.5.1 UV Raman Microspectrometer for CVD Diamond Studies

Figure 2.1 illustrates the optical layout of the microspectrometer. We utilize a modified Olympus U-RLA microscope with an epi-illuminator and a universal lamp housing. The excitation beam is introduced to the sample independently of the light collection optics, as opposed to the more typical epi-illumination. Our design has the advantage that the beam focal spot size and position are adjustable independently of the focusing conditions for collecting the Raman scattered light. In addition, since we use a Cassegrain objective, the prism in front of the objective does not obscure either the excitation beam or collected scattered light.

We utilize an intracavity frequency doubled argon ion laser to excite the UV Raman scattering [23]. For many of these experiments we utilized 244 and 229 nm excitation. The CW UV Raman laser beam is expanded to a ~ 10 mm

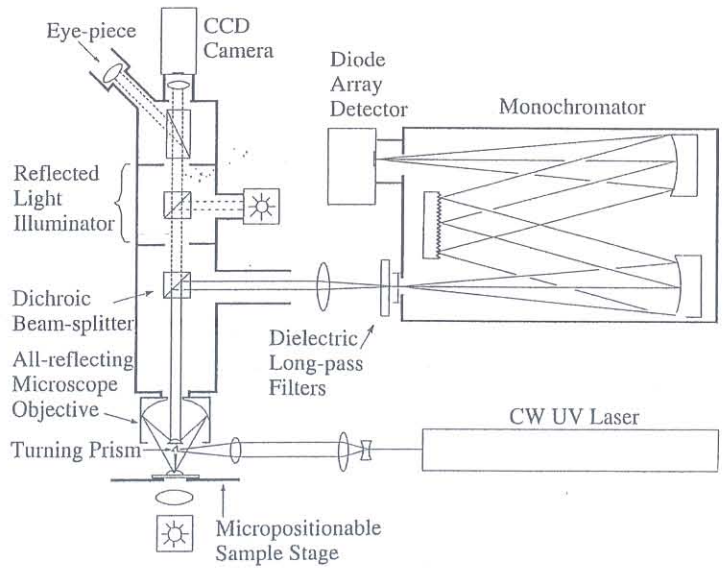

Fig. 2.1. Schematic showing the optical layout of the UV Raman microspectrometer

diameter and focused using a 5–10 cm focal-length lens onto the sample via a Suprasil 90° turning prism mounted directly below the Cassegrain objective. The beam can be focused to a spot size of 5–25 μm. An Opticon Corp. 36× all-reflective Cassegrain microscope objective with a back focus of 160 mm, a working distance of 10.5 mm and a numerical aperture (N.A.) of 0.5 is used to collect the backscattered light. The 0.5 N.A. objective enables collection of scattered radiation over a large solid angle (half angle = 30°). The objective has a dielectric over-coated aluminum coating (Al/MgF_2). This Cassegrain objective serves as a highly efficient collection optic for the scattered radiation: Collecting at $f/1$, the sample spot size of 5–10 μm can be imaged efficiently into the entrance slit (100–200 μm) of the monochromator ($f/6.8$).

An Omega Optical Inc. 290 DCLPO2, UV dichroic beam splitter was used to reflect > 90% of the scattered UV light between 230 and 265 nm towards the collecting optics of the monochromator and to transmit light between 300 and 2000 nm to the microscope trinocular eyepiece. The dichroic beam splitter is mounted in a fluorescence cube module, housed in the epi-illuminator turret that was modified to enable the efficient coupling of the scattered UV radiation into the spectrograph.

A 0.75 m single monochromator ($f/6.8$) was used to disperse the scattered light. We utilized two dielectric longpass filters, custom constructed by Omega Optical Inc. with a transmittance of 0.01% at 244 nm and 65–80% between 252 nm and 262 nm to reject the Rayleigh scattered light.

We earlier demonstrated that diamond Raman spectra excited within or close to the diamond bandgap have dramatically improved S/N ratios, due to the lack of interfering fluorescence signals [34–36]. This allowed us to monitor the spectral differences between different non-diamond carbon species. We were also able to observe for the first time the carbon-hydrogen (C – H) stretching vibrations of the non-diamond components of CVD diamond films and to examine the intensity and frequency of the third-order phonon bands of diamond. Furthermore, we were able to detect and quantify different non-diamond carbon species in the CVD diamond films.

Figure 2.2 shows the surface of the (100) face of a diamond crystallite which occurs on the surface of a CVD diamond film, while Fig. 2.3 shows the UV Raman spectra of this CVD diamond film excited at 244 nm (~ 1.5 mW). The diamond UV Raman spectra were recorded with the laser spot centered on the (100) face of this single diamond crystallite (Fig. 2.3a), or at the grain boundaries between diamond crystallites (Fig. 2.3b).

The absolute intensity of the diamond first order phonon band at 1332 cm^{-1} was approximately the same at the (100) face (Fig 2.3a)and at the grain boundaries (Fig 2.3b). However, the UV Raman spectrum taken from the grain boundaries showed a broad band at ~ 1600 cm^{-1}, assignable to non-diamond carbon impurities. This band was not present in the spectrum from the (100) crystallite face. These results demonstrate the ability to determine the spatial distribution of non-diamond impurities in CVD diamond films.

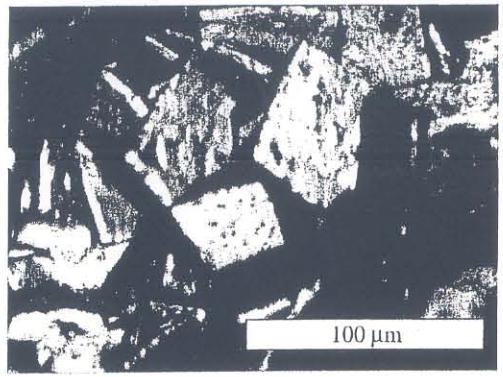

Fig. 2.2. CVD diamond film surface viewed with visible light epi-illumination through the microscope attachment of the UV Raman microspectrometer, showing the (100) faces of single crystallites

Our previous study of the oxidative degradation of CVD diamond films showed that upon oxidation the intensity of the broad non-diamond carbon

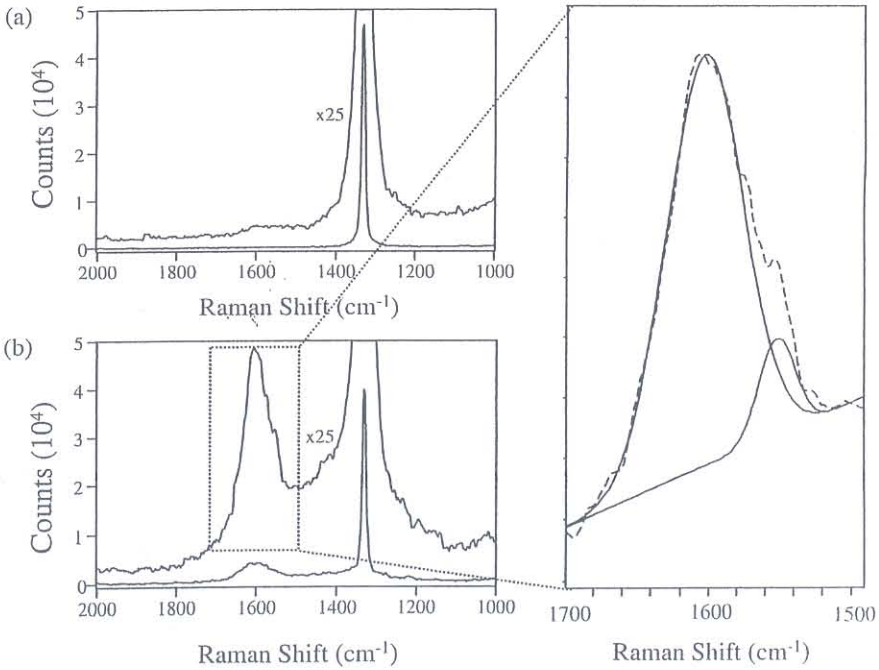

Fig. 2.3. (a) Raman spectra from CVD diamond film of the (100) face of a single crystallite, and (b) at the interstices between diamond crystallites (244 nm: ~ 1.5 mW average power: 10 s total accumulation time: 100 μm entrance slit)

band at $\sim 1550\,\mathrm{cm}^{-1}$ and the C – H stretching band of the non-diamond components at $2930\,\mathrm{cm}^{-1}$ decreased with respect to the diamond first order phonon band, but that the initial rate of decrease was significantly greater for the $1550\,\mathrm{cm}^{-1}$ band than for the $2930\,\mathrm{cm}^{-1}$ band [34–36]. These results indicate that non-diamond carbon species are oxidized in preference to diamond. They also suggest that more than one non-diamond carbon impurity is present in CVD diamond films.

Figure 2.3b illustrates that by using UV Raman microspectrometry we can resolve underlying components of the non-diamond carbon band. In this instance, a sharp low energy feature, fitted to the $\sim 1553\,\mathrm{cm}^{-1}$ amorphous carbon band, is resolved from the broad $\sim 1603\,\mathrm{cm}^{-1}$ non-diamond carbon band. In other instances, the sharp $\sim 1580\,\mathrm{cm}^{-1}$ graphite band dominates the non-diamond carbon band. The limited spatial area probed enables us to speciate the different non-diamond carbon species that make up the normally broad non-diamond carbon band.

2.5.2 UV Raman Instrument for in situ Studies of CVD Diamond Growth

A UV Raman spectrometer [38] was constructed to examine *in situ* the growth of diamond in a microwave plasma CVD diamond reactor (Fig. 2.4). We utilized a 1.5 kW ASTeX microwave plasma reactor that was modified with silica viewports for spectroscopic access to the growing films during deposition. The *in situ* UV Raman spectra were excited with CW 244 nm light from a Coherent Innova 300 intracavity frequency doubled argon ion laser. The 244 nm output was expanded and focused through a silica viewport and onto the growth substrate/sample inside the reactor.

The scattered light was collimated by using a 90° off-axis parabolic mirror. Two 244 nm dielectric stack filters were used to reject Rayleigh scattering. The filtered Raman scattered light was reimaged onto the slit of a modified Spex 1701, 0.75 m single monochromator (f/6.8) equipped with a 2400 groove/mm holographic grating, and an EG&G PARC 1456 blue intensified photodiode array optical multichannel analyzer. A spatial filter (600 µm aperture) was incorporated into the collection optical train directly behind the spectrograph entrance slit to limit the measured sample volume by approximating confocal imaging. Approximate confocal imaging was used to help minimize interference from the plasma emission in the reactor. Although the plasma emission intensity in the visible is sufficiently high to prevent visible wavelength Raman measurements, it decreases dramatically in the UV spectral region below ~ 260 nm.

Figure 2.5 shows the *in situ* temperature dependence of the first order Raman band of the growing diamond films ($\sim 1332\,\mathrm{cm}^{-1}$ at room temperature). We see very high S/N spectra for relatively short ~ 10 min spectral accumulation times. The independently measured plasma emission (measured in the absence of the excitation beam) is easily subtracted off. We calculate

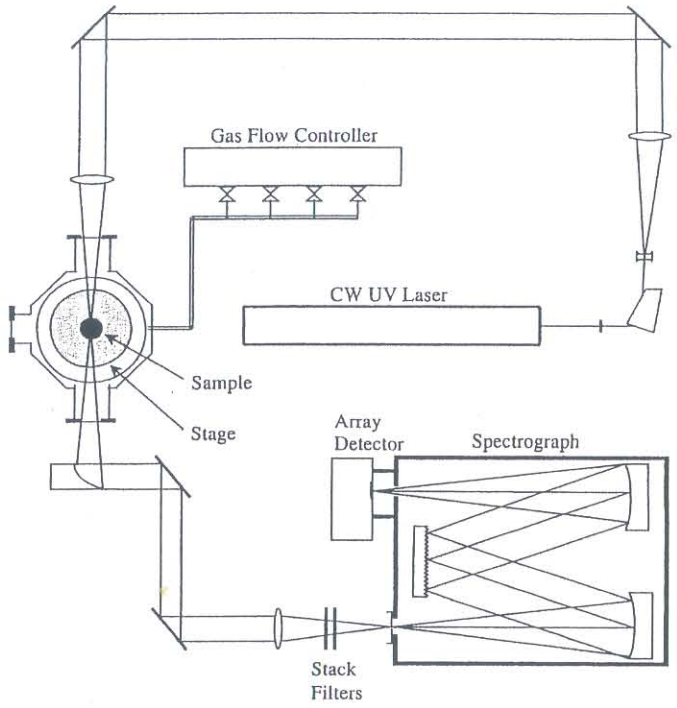

Fig. 2.4. Schematic diagram showing the UV Raman spectrometer coupled to the ASTex plasma CVD diamond growth chamber

an ~ 8 Å thickness *in situ* detection limit for the growing CVD diamond films within the plasma reactor.

The spectra display the well known frequency decrease of the first order phonon band with temperature. This band frequency can be independently used for determining temperature. We were surprised not to observe the expected nondiamond carbon impurity bands in these spectra, since they were clearly observed in spectra of these same CVD films when they were cooled down to room temperature. To our surprise we discovered that these non-diamond carbon bands are enhanced by a narrow electronic resonance at ~ 244 nm whose frequency is temperature dependent. This electronic resonance shifts away from this 244 nm excitation wavelength at elevated temperatures such that the Raman intensity is significantly decreased. Future experiments will use adjacent UV excitations such as 229 or 238 nm to examine these nondiamond carbon bands at the elevated temperatures required for CVD diamond growth.

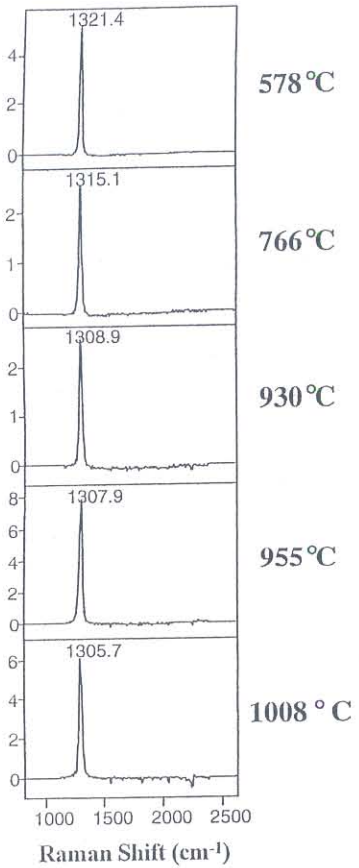

Fig. 2.5. Temperature dependence of the in situ 244 nm UV Raman spectra of CVD diamond films grown within the plasma reactor

2.6 Conclusions

These are only two examples of the development of Raman instrumentation for material science applications. These examples, show that Raman spectroscopy is a uniquely powerful probe of the underlying properties of materials and molecular structure of the constituents. The technique measures both vibrational frequencies and intensities. The frequencies report on chemical bonding, molecular structure and environment. The intensities monitor the strength of coupling between vibrational and electronic motion in the material. The spectra obviously have an extraordinarily high information content. Future instrument improvements will further enable the growth and adaptations of Raman spectroscopy to a variety of new applications. The new generations of Raman spectrometers are compact, highly efficient and highly adaptable instruments. This is a very exciting time to be working in the field of Raman spectroscopy.

References

1. L.A. Lyon, C.D. Keating, A.P. Fox, B.E. Baker, L. He, S.R. Nicewarner, S.P. Mulvaney, M.J. Natan: Anal. Chem. **70**, 341R (1998)
2. M. Delhaye, J. Barbillat, J. Aubard, M. Bridoux, E. Da Silva: in *Raman Microscopy: Developments and Applications*, ed. by G. Turrell, J. Corset (Academic, London 1996)
3. R.L. McCreery: *Modern Techniques in Raman Spectroscopy, Instrumentation for Dispersive Raman Spectroscopy*, ed. by J.J. Laserna (Wiley, New York 1996). pp. 41–72
4. Photonics Spectra **66** (December 1998)
5. (a) J. Ma, Y.S. Li: Appl. Opt. **35**, 2527 (1996) (b) S.E. Nave: ISA, **96**, 453 (1996)
6. D.A. Long: *Raman Spectroscopy* (McGraw-Hill, New York 1977); D.P. Strommen, K. Nakamoto:*Laboratory Raman Spectroscopy* (Wiley, New York 1984)
7. S.A. Asher: Ann. Rev. Phys. Chem. **39**, 537 (1988)
8. J.M. Dudik, C.R. Johnson, S.A. Asher: J. Chem. Phys. **82**, 1732 (1985)
9. D.B. Chase, J.F. Rabolt:*Fourier Transform Raman Spectroscopy* (Academic, New York 1994)
10. S.A. Asher, C.R. Johnson: Science **225**, 311 (1984)
11. S.A. Asher, C.H. Munro, Z. Chi: Laser Focus World, 99 (1997)
12. (a) S.A. Asher: Anal. Chem. **65**, 59A-66A (1993) (b) S.A. Asher: Anal. Chem. **65**, 201A (1993)
13. M. Sparrow, W. Hug, S.A. Asher: Appl. Spectrosc., in preparation (1999)
14. T.C. Strekas, T.G. Spiro: Biocim. Biophys. Acta **263**, 830 (1972)
15. M.D. Levinson: *Introduction to Non Linear Laser Spectroscopy* (Academic Press, New York (1982)
16. J. Teraoka, P.A. Harmon, S.A. Asher: J. Am. Chem. Soc. **112**, 2892 (1990)
17. P.A. Harmon, J. Teraoka, S.A. Asher: J. Am. Chem. Soc. **112**, 8789 (1990)
18. T.F. Cooney, H.T. Skinner, S.M. Angel: Appl. Spectrosc. **49**, 1846 (1995)
19. C.M. Jones, V.L. Devito, P.A. Harmon, S.A. Asher: Appl. Spectrosc. **41**, 1268 (1987)
20. S.A. Asher, C.R. Johnson, J. Murtaugh: Rev. Sci. Instr. **54**, 1657 (1983)
21. B. Hudson, R.J. Sension, R.J. Brudzynski, S. Li:*Proceedings of the XI International Conference on Raman Spectroscopy*, ed. by R.H. Clark, D.A. Long (Wiley, New York 1988)
22. (a) S.A. Asher, Z. Chi, J.S.W. Holtz, I.K. Lednev, A.S. Karnoup, M.C. Sparrow: J. Am. Chem. Soc. **121**, 4076 (1999) ; (b) I.K. Lednev, A.S. Karnoup, M.C. Sparrow, S.A. Asher: J. Am. Chem. Soc. **121**, 8074 (1999)
23. S.A. Asher, R.W. Bormett, X.G. Chen, D.H. Lemmon N. Cho, P. Peterson, M. Arrigoni, L. Spinelli, J. Cannon: Appl. Spectrosc. **47**, 628 (1993)
24. J.S.W. Holtz, R.W. Bormett, Z. Chi, N. Cho, X.G. Chen, V. Pajcini, S.A. Asher, L. Spinelli, P. Owen, M. Arrigoni: Appl. Spectrosc. **50**, 1459 (1996)
25. C.L. Schoen, S.K. Sharma, C.E. Helsley, H. Owen: Appl. Spectrosc **47**, 305 (1993)
26. P.L. Flaugh, S.E. O'Donnell, S.A. Asher: Appl. Spectrosc. **38**, 847 (1984)
27. See e.g. [3] or [6]
28. M. Futamata: Appl. Spectrosc. **50**, 199 (1996)
29. C.H. Munro, V. Pajcini, S.A. Asher: Appl. Spectrosc. **51**, 1722 (1997)

30. B.G. Bovard: Appl. Opt. **32**, 5427 (1993)
31. H.R. Morris, C.C. Hoyt, P. Miller, P.J. Treado: Appl. Spectrosc **50**, 805 (1996)
32. B. Chase: Appl. Spectrosc. 48, 14A (1994)
33. Y. Narita, T. Tadokoro, T. Ikeda, T. Saiki, S. Mononobe, M. Ohtsu: Appl. Spectrosc. **52**, 1141 (1998)
34. C.D. Zuiker, A.R. Krauss, D.M. Gruen, J.A. Carlisle, L.J. Terminello, S.A. Asher, R.W. Bormett: Mat. Res. Soc. Symp. Proc. **437**, 211 (1996)
35. R.W. Bormett, S.A. Asher, R.E. Witkowski, W.D. Partlow, R. Lizewski, F. Pettit: J. App. Phys **77**, 5916 (1995)
36. V.I. Merkulov, J.S. Lannin, C.H. Munro, S.A. Asher, V.S. Veerasamy, W.I. Milne: Phys. Rev. Lett. **78**, 4869 (1997)
37. V. Pajcini, C.H. Munro, R.W. Bormett, R.E. Witkowski, S.A. Asher: Appl. Spectrosc. **51**, 81 (1997)
38. J.C. Worthington, R.W. Bormett, C.H. Munro, R.E. Witkowski, S.A. Asher: in *Proc. XV International Conf. on Raman Spectrosc.*, ed. by S.A. Asher, P. Stein (John Wiley, 1996) p. 1218